Enhanced Stability of Monomer Fold Correlates with Extreme Drug Resistance of HIV-1 Protease

John M. Louis,*[†] József Tözsér,[‡] Julien Roche,[†] Krisztina Matúz,[‡] Annie Aniana,[†] and Jane M. Sayer[†]

[†]Laboratory of Chemical Physics, National Institute of Diabetes and Digestive and Kidney Diseases, National Institutes of Health, DHHS, Bethesda, Maryland 20892, United States

[‡]Department of Biochemistry and Molecular Biology, Faculty of Medicine, University of Debrecen, Debrecen H-4012, Hungary

ABSTRACT: During treatment, mutations in HIV-1 protease (PR) are selected rapidly that confer resistance by decreasing affinity to clinical protease inhibitors (PIs). As these unique drug resistance mutations can compromise the fitness of the virus to replicate, mutations that restore conformational stability and activity while retaining drug resistance are selected on further evolution. Here we identify several compensating mechanisms by which an extreme drug-resistant mutant bearing 20 mutations (PR20) with >5-fold increased K_d and >4000-fold decreased affinity to the PI darunavir functions. (1) PR20 cleaves, albeit poorly, Gag polyprotein

substrates essential for viral maturation. (2) PR20 dimer, which exhibits distinctly enhanced thermal stability, has highly attenuated autoproteolysis, thus likely prolonging its lifetime in vivo. (3) The enhanced stability of PR20 results from stabilization of the monomer fold. Both monomeric PR20$_{T26A}$ and dimeric PR20 exhibit T_m values 6−7.5 °C higher than those for their PR counterparts. Two specific mutations in PR20, L33F and L63P at sites of autoproteolysis, increase the T_m of monomeric PR$_{T26A}$ by ∼8 °C, similar to PR20$_{T26A}$. However, without other compensatory mutations as seen in PR20, L33F and L63P substitutions, together, neither restrict autoproteolysis nor significantly reduce binding affinity to darunavir. To determine whether dimer stability contributes to binding affinity for inhibitors, we examined single-chain dimers of PR and PR$_{D25N}$ in which the corresponding identical monomer units were covalently linked by GGSSG sequence. Linking of the subunits did not appreciably change the ΔT_m on inhibitor binding; thus stabilization by tethering appears to have little direct effect on enhancing inhibitor affinity.
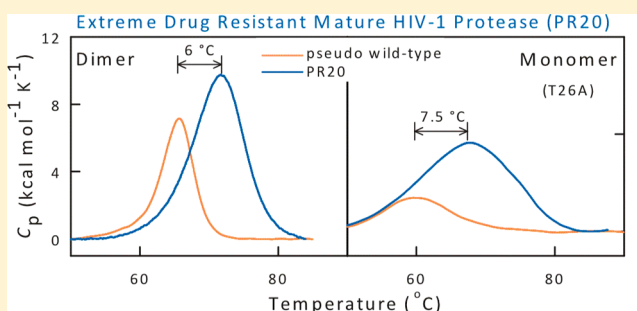
The protease (PR) of HIV-1 is indispensable for processing the retroviral Gag and Gag−Pol polyproteins to release the structural and functional proteins essential for maturation and propagation of an infectious virus. PR is one of the primary targets for antiviral therapy and several potent protease inhibitors (PIs) have been developed for clinical use. Encoded as part of the viral Gag−Pol polyprotein, PR mediates its own release by a multistep autocatalytic process (autoprocessing).[1−4] A crucial step in this process is the cleavage at the N-terminus of the PR domain, accompanied by appearance of catalytic activity and stable dimer formation.[3] The mature PR is a homodimer consisting of two 99-amino acid monomer units each of which contributes one aspartyl residue to the active site, part of the conserved active site interface triad Asp−Thr−Gly.[5] Other regions contributing to the dimer interface are the flaps, which adopt a closed conformation upon binding of a substrate or inhibitor, and the four-stranded antiparallel β-sheet, comprising the four N- and C-terminal strands of the two monomers, which play a major role in holding the subunits together.[6] Several PIs, 8−10 of which are in widespread current use,[7] have been designed to bind to the active site of the PR dimer at low nanomolar and picomolar affinities. However, the noteworthy success of these drugs is accompanied by a serious drawback, because error-prone replication by the virally

encoded reverse transcriptase facilitates the rapid emergence of drug resistant mutants (DRMs), selected in the presence of PIs as functionally competent enzymes. Some of these highly evolved PR variants contain multiple mutations and are resistant to most, if not all, PIs.[8,9]

In addition to major DRMs, which directly affect substrate and/or inhibitor binding, so-called accessory or compensatory mutations remote from the active site, some of which correspond to naturally occurring variants,[10] are frequently observed to coevolve with the major mutations. These polymorphisms may pre-exist or they may evolve after emergence of major DRM(s) under drug pressure, and they are selected because they confer functional advantages to the drug resistant PR. Structural studies to date have focused on mechanisms whereby long-range effects of distal mutations alter the conformation of the binding site and/or flaps, and consequently, the energetics of inhibitor binding.[11−13] Some of these mutations in PR also partially restore the biological fitness of the mutant virus to replicate, which is adversely

affected by major DRMs.[14−16] Accessory mutations such as L10I, L63P, and A71V have been shown to increase the thermal stability and pH tolerance of a drug resistant PR bearing the destabilizing active-site mutation I84V.[17] Several drug resistant PRs bearing both active-site and remote mutations exhibit thermal stability exceeding that of the wild-type dimer. These include ANAM-11,[11] which bears 11 mutations including L63P, and mutant I50L/A71V showing T_m increases of 4.8 °C and ∼2 °C, respectively, relative to the wild type.[18] In the present study, we describe the basis for enhanced thermal stabilization of a highly drug resistant mutant protease, PR20, which to our knowledge has the highest such thermal stabilization (as well as the largest number of mutations) for a drug resistant PR observed to date.

PR20, a clinical isolate first reported by Dierynck et al.,[19] bears 20 amino acid substitutions both near and remote from the active site. Mature PR20 exhibits a 3−4 orders of magnitude decreased affinity for PIs darunavir (DRV) and saquinavir, relative to the wild type PR. Furthermore a model precursor (TFR-PR20) in which the protease is flanked at its N-terminus by the transframe region (TFR) of Gag−Pol, undergoes efficient autoprocessing to release the TFR and PR20, in the presence of every clinical PI including darunavir (DRV) up to 250 μM concentration.[9] By contrast, the processing of the corresponding wild-type precursor is inhibited by DRV with an IC_{50} of ∼1 μM. These observations account for the viability of HIV-1 with mutant PR20, which successfully evades inhibition even by highly effective second generation PIs. In the present study, we examine the kinetic parameters of PR20 using a chromogenic substrate, its monomer−dimer equilibrium, and urea induced unfolding. Next, using differential scanning calorimetry, we investigate several properties relating to the stability of PR20 such as (1) whether the enhanced stability of PR20 relative to PR results from intermonomer interactions or a more stable monomer fold, (2) if specific mutations L33F and L63P at sites of autoproteolysis selected under drug pressure in PR20 affect both autoproteolysis and stability, and (3) whether an entropically stabilized PR dimer as a single-chain construct influences binding affinity to inhibitors. Finally, we explore the relative catalytic efficiencies of PR20- and PR-mediated hydrolysis of peptide substrates corresponding to natural sites in Gag polyprotein to help understand if hyper-resistance is associated with selection for cleavage of some substrates different in their order of efficiencies as compared to wild-type PR.

■ MATERIALS AND METHODS

Protein Expression and Purification. Previously reported constructs used in this study are PR,[20] PR20,[9,19] ANAM-11,[9,11] PR$_{D25N}$,[21] and PR$_{T26A}$.[22] Constructs used for the first time are PR20$_{K7Q}$, PR20$_{T26A}$, PR$_{L33F/L63P}$, PR$_{T26A/L33F/L63P}$, PR$_{L33F/E34D/L63P}$, ScPR, and ScPR$_{D25N}$. Genes were synthesized and cloned in a pET11a vector between Nde1 and BamH1 sites and transformed into *Escherichia coli* BL-21(DE3). Substitution mutations were introduced using the Quik-Change mutagenesis kit reagents and protocol (Agilent Technologies) and verified by DNA sequencing. Cells bearing the corresponding plasmid were grown at 37 °C either in Luria−Bertani medium or in a modified minimal medium with ^{15}N ammonium chloride and ^{13}C glucose as the sole nitrogen and carbon sources. Induction for protein expression, isolation of inclusion bodies, and purification were carried out as described previously.[23,24]

Proteins were subjected to electrospray ionization mass spectrometry (ESI-MS) to verify composition prior to use. Proteins were folded freshly as described, either by the dialysis or by the quench protocol[25] for enzyme kinetics, calorimetric and NMR studies.

Spectrophotometric Enzyme Assays. Enzymatic activity was measured at 28 °C with chromogenic substrate IV [Lys-Ala-Arg-Val-Nle-(4-NO$_2$Phe)-Glu-Ala-Nle-NH$_2$, California Peptide Research, Napa, CA] by following the decrease in absorbance at 310 nm in 50 mM sodium acetate buffer, pH 5, containing 250 mM sodium chloride. The protease was folded by the quench protocol to a final concentration of 0.5 μM as described,[25] and reactions were initiated by the addition of substrate. Absorbance change was converted to molarity by the use of $\Delta\varepsilon$ = 1797 M^{-1} cm^{-1}, and the data at substrate concentrations from 72 to 430 μM were analyzed with the enzyme kinetics module of SigmaPlot 10 (Systat Software, Inc.). The dimer dissociation constant, K_d, was measured under the same conditions at a substrate concentration of 430 μM and varying concentrations of PR20 from 0.026 to 1.9 μM (as monomers). An equation previously described[24] was used to fit the data. The effect of up to 2.4 M urea on the rate of substrate (400 μM) hydrolysis by 0.53 μM PR20 was measured at the same pH and NaCl concentration as above (pH of urea stock solution adjusted to 5.07).

Fluorescence Measurements. The effect of urea on the intrinsic fluorescence of PR20 was measured by use of a Fluoromax-3 spectrofluorometer (Horiba Jobin Yvon, Edison, NJ) with excitation and emission wavelengths of 285 and 350 nm, respectively, and a bandwidth of 2 nm. The method, based on a previously described protocol,[25] consisted of replacing successive 70 μL aliquots of the measured solution (1 mL of 1 μM folded PR20 in 50 mM sodium acetate, pH 5, initially containing no urea) with an equal volume of a solution of the same composition containing 3.6 M urea to reach a final urea concentration of 2.2 M. The fluorescence signal was recorded upon reaching a stable end point after each successive replacement. A second experiment followed the same procedure with 2 μM DRV in both solutions.

NMR Experiments. [1]H−^{15}N TROSY-HSQC spectra were recorded at 293 K on a uniformly [15]N- and ^{13}C-labeled sample at 100 μM protein concentration in 20 mM sodium acetate buffer, pH 5.8, using a 600 MHz Bruker Avance II spectrometer equipped with a z-axis TCI cryogenic probe. The 512* × 1024* complex points in the indirect and direct dimensions were collected for acquisition times of 266 (t_1) and 122 (t_2) ms. The interscan delay was set to 1.5 s. The spectra were processed using NMRPipe[26] and displayed with SPARKY.[27]

Differential Scanning Calorimetry. Proteins were folded from 7 or 12 mM HCl by a quench protocol as previously described,[25] to give a final pH of 5.0 in 50 mM acetate or 3.6 in 25 mM formate buffers (Table 1). To avoid possible precipitation at higher buffer concentrations, scPR$_{D25N}$ (with and without inhibitor) was folded by addition of 5.66 volumes of 5 mM sodium acetate buffer, pH 6.0, to 1 volume of protein in 12 mM HCl (final pH 4.7). For experiments in the presence of DRV or RPB, the inhibitor (∼2-fold molar excess relative to dimers) was added in the folding buffer. DSC measurements were performed by using a MicroCal VP-DSC microcalorimeter (GE Healthcare), and data were analyzed with the instrument's Origin software.[21]

Kinetics Using Peptides Representing Natural Sites of Polyprotein Processing. Assays with peptides incorporating

Table 1. DSC Data[a] and Dimer Dissociation Constants (K_d) for Selected PR Constructs

(A)			
protein	T_m (−DRV)	T_m (+DRV)	ΔT_m (I)[b]
PR	65.7[c]	88.1[c]	22.4
PR$_{L33F/E34D/L63P}$	nd[d]	85.4	
PR20[e]	71.7	77.0	5.3
ANAM-11[e]	70.5	81.9	11.4
PR$_{T26A}$	60.0	63.0	3.0
PR20$_{T26A}$	67.5	67.5	0
PR$_{T26A/L33F/L63P}$	68.1	67.1	−1.0

(B)				
protein	T_m	T_m	ΔT_m (I)[b]	ΔT_m (Sc)[f]	K_d (μM)
	(−RPB)	(+RPB)			
PR[g]	56.6	65.8	9.2	11 (−RPB)	<0.01[c]
ScPR[g]	67.6	75.4	7.8	9.6 (+RPB)	
	(−DRV)	(+DRV)			
PR$_{D25N}$	58.4[c]	61.5[c]	3.1	9.0 (−DRV)	1.3[c]
ScPR$_{D25N}$	67.4	70.3	2.9	8.8 (+DRV)	

[a]At pH 4.7–5.0 in sodium acetate buffer unless noted otherwise. [b]T_m(+inhibitor) − T_m(−inhibitor). [c]Cited from ref 21; an approximately 100-fold increase in K_d observed based on the active site mutation D25N in PR accompanies ~10^6-fold weaker binding of DRV. [d]nd (not determined) due to more rapid autoproteolysis than that for PR (Figure 2). [e]Reference 9. [f]T_m(single chain) − T_m(homodimer). [g]In 25 mM sodium formate, pH 3.6.

natural cleavage sites in Gag were initiated by mixing 5 μL (50–14000 nM) of purified PR20 or 5 μL (9–350 nM) of purified PR with 10 μL 2× of incubation buffer (0.5 M potassium phosphate buffer, pH 5.6, containing 10% glycerol, 2 mM ethylenediaminetetraacetic acid (EDTA), 10 mM dithiothreitol, 4 M NaCl), and 5 μL (0.1–6 mM) of substrate dissolved in water (or, in the case of Met-containing peptides, in 10 mM DTT). After incubation at 37 °C for 1 h, the reaction was terminated by the addition of 180 μL of 1% trifluoroacetic acid. Substrates and cleavage products were separated using a reverse-phase HPLC method described previously.[28] Kinetic parameters were determined by fitting data obtained at less than 20% substrate hydrolysis to the Michaelis−Menten equation by use of SigmaPlot software. The experimental errors of the determined parameters were smaller than 25%. The amount of active proteases used in the assays was determined by active site titration using the potent HIV-1 PR inhibitor amprenavir. Active-site titration was performed using the HPLC method, except 0.2 μL aliquots of the inhibitor (0–10 μM) were added to the reaction mixture.

■ **RESULTS AND DISCUSSION**

Figure 1A shows a schematic representation of the Gag and Gag−Pol polyproteins and the order in which the protease-catalyzed cleavage steps in their processing occur. In Figure 1B, the amino acid sequence of PR20[19] is aligned with the wild-type enzyme (PR^{wt}) and with an optimized construct, designated as PR.[4,20,29] We have shown previously that substituting the Cys residues to Ala does not alter the conformational stability or the kinetic parameters of PR and facilitates sample handling for NMR experiments.[4,20] Mutations defined as major DRMs associated with DRV and saquanvir (SQV) resistance are 147V, I54L, I84V (DRV), and L90M (SQV).[7] A recent crystallographic study has revealed novel flap

conformations and an expanded inhibitor binding site for PR20[13] and relates its reduced inhibitor binding affinity to propagation of structural changes resulting from the distal "accessory" mutations. The structure shown in Figure 1C represents a superimposition of PR20 (3UCB[13]) on PR (2IEN[30]), showing the location of the 20 mutations present in PR20. The present study focuses on the mechanism(s) by which such mutations also contribute to structural stabilization and function of the PR.

Kinetic and Biochemical Characterization of PR20. PR^{wt} (Figure 1B) undergoes rapid and substantial self-cleavage (autoproteolysis) concomitant with loss of activity upon folding and incubation under optimal conditions, which may constitute a mechanism for down-regulation of PR activity.[20] To overcome this problem, a construct was designed bearing mutations Q7K, L33I, and L63I at residues at or near the three major sites of autoproteolysis.[20,29] Autoproteolysis of this construct was markedly reduced even after incubation for 11 days at 5−10 μM, pH 5.5 and 25 °C.[29] Incubation of 13 μM PR (which also includes C67A and C95A substitutions, Figure 1B) for 23−70 h at room temperature in 50 mM sodium acetate buffer, pH 5, resulted in a small, time dependent appearance of products of autoproteolysis (Figure 2A, bands marked P). By contrast, incubation of PR20 for up to 115 h under the same conditions revealed essentially no lower mass cleavage products (Figure 2B). We speculate that attenuation of autoproteolysis may contribute to the longevity of PR20 in vivo, thus possibly compensating for its decreased catalytic efficiency (k_{cat}/K_m, see below). It is likely that attenuated autoproteolysis of PR20 is favored by specific mutations influencing the catalytic machinery of PR20.

It is noteworthy that the major site of autoproteolysis between Leu5/Trp6[4,29] in PR20 does not contain naturally selected mutations flanking 4 residues on either side (P/P′) of this site including K7[19] unlike the other two sites (L33/E34 and L63/I64, Figure 1B). To ascertain that the Leu5/Trp6 site is not a preferred site for autoproteolysis, we created a revertant bearing K7Q mutation (wild-type site) in PR20. Incubation of folded PR20$_{K7Q}$ showed no loss in catalytic activity over a period of 25 h (Figure 2E) and analysis by SDS-PAGE even after 48 h also failed to show significant products corresponding to cleavage of this site (Figure 2C). However, by ESI-MS we were able to detect a very small fraction of the protein (<5%) corresponding only to the product spanning protease residues 6−99 after 48 h. Products corresponding to the cleavage at the other two sites are absent in PR20$_{K7Q}$, similar to PR20. These results clearly indicate that the 19 mutations selected in PR20 under drug pressure naturally suppress the Leu5/Trp6 cleavage without additional substitutions at P/P′ positions, different from L33/E34 and L63/I64 sites. We chose to retain the Q7K mutation as all our previous studies were carried out with this mutation, thus enabling a strict comparison with our present PR20 data on its characterization. Notably, biochemical and structural studies are unreliable to carry out without this substitution in the wild-type protease because of rapid autoproteloysis leading to dimer dissociation and loss of catalytic activity,[4,20] and the mutation Q7K is not expected to influence autoproteolysis at L33/E34 and L63/I64 sites, which is indeed our focus.

Hydrolysis by PR20 of a chromogenic substrate based on the Gag CA/SP1 cleavage site, substrate IV, exhibits Michaelis−Menten kinetics, with an estimated K_m higher than concentrations that can be used, because of substrate inhibition
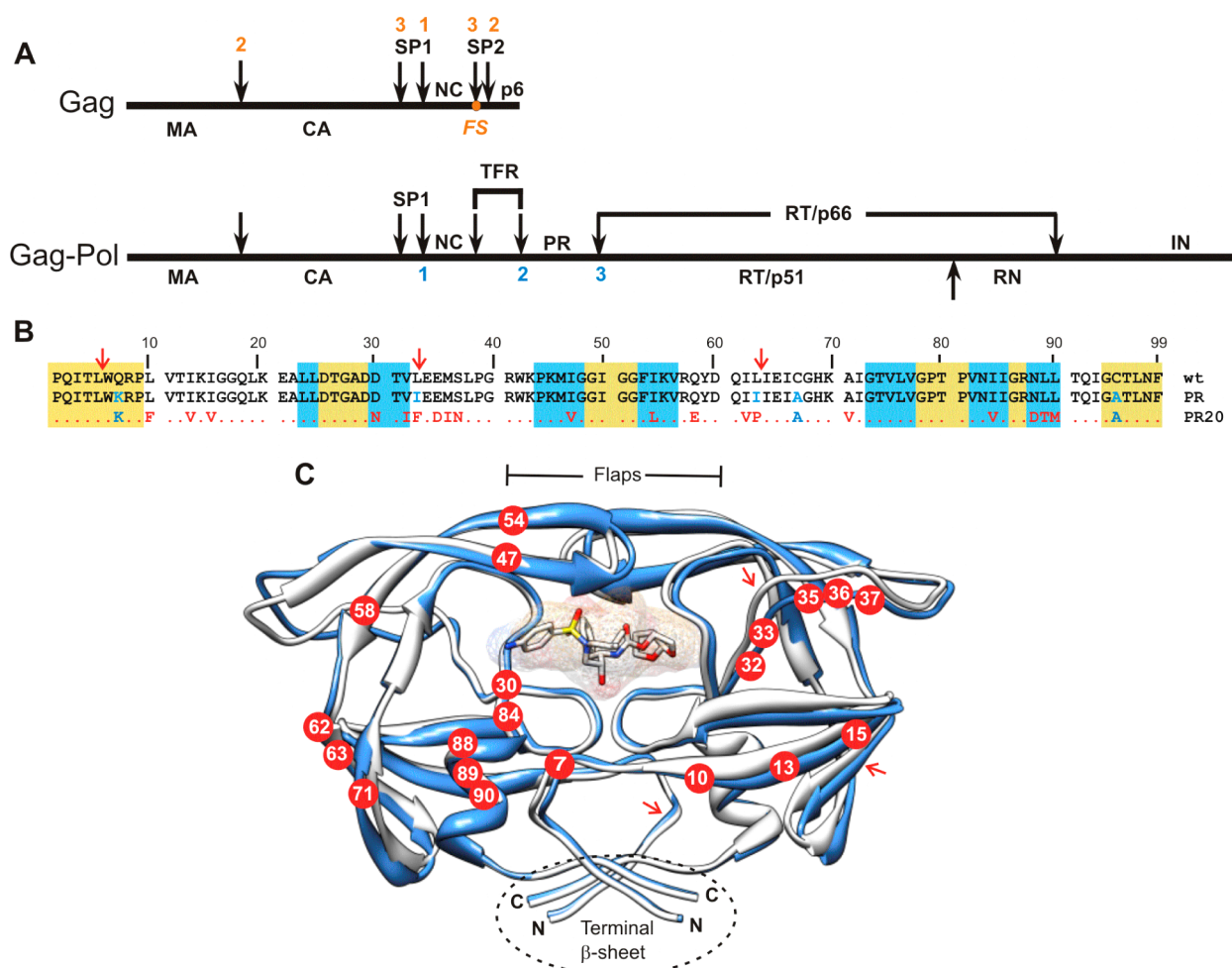
Figure 1. (A) Organization of Gag and Gag−Pol polyproteins of HIV-1. Nomenclature of domains in Gag:[2] MA, matrix; CA, capsid; SP1, spacer peptide 1; NC, nucleocapsid; SP2, spacer peptide 2. In Gag−Pol: TFR, transframe region; PR, protease; RT, reverse transcriptase; RN, Rnase H; IN, integrase. FS designates the location of the −1 frame shift during translation that results in production of Gag−Pol. Numbers shown above (red) and below (blue) the schematic lines designate the order in which sequential cleavages occur in Gag and in Gag−Pol, respectively.[2,9] (B) Sequence alignment of PR20 with wild-type HIV-1 protease (PR[wt]) and its optimized mutant (termed PR). Residues in PR and PR20 shown in blue were introduced to limit autoproteolysis and to preclude cysteine−thiol oxidation. Residues shown in red are natural mutations in the clinical isolate from which PR20 is derived.[19] The gold and white backgrounds indicate highly conserved regions in the protease domain in drug treated patients,[41] and areas of greatest variability among isolates, respectively. The blue background designates regions where major DRMs (as defined in http://hivdb.stanford.edu/cgi-bin/PIResiNote.cgi) occur. (C) Ribbon representation (blue) of PR20 in complex with DRV (pdb accession code 3UCB[13]) superimposed on PR (white, pdb accession code 2IEN[30]). Locations of the mutations in PR20 are shown as red circles with residue numbers in white. The DRV inhibitor is shown as a stick and surface representation in the active site cavity. Major sites of autoproteolysis are indicated in (B) and (C) with red arrows. Molecular representations were prepared using Chimera.[42]

above 500 μM (Figure 3A). Kinetic parameters $K_m = 617 \pm 84$ μM and $k_{cat.} = 215 \pm 19$ μM min^{-1} at pH 5 and 250 mM NaCl were estimated by curve fitting to the acquired kinetic data (see also Lineweaver−Burke plot, Figure 3A inset). A low value of $k_{cat.}/K_m$ for PR20, roughly an order of magnitude smaller than that for PR under the same conditions (Figure 3B),[31] thus appears to be largely a consequence of the high K_m rather than a decreased $k_{cat.}$. Compromised substrate binding correlates with the open flap conformations evident in PR20 crystal structures.[13] In particular, PR20 has five mutations between residues 32 and 37 in or near the flap hinge region that can account for different flap orientations. Another multidrug resistant mutant, MDR769 (PDB accession code ITW7),[12] which exhibits a pronounced "wide-open" conformation of both flaps, also contains several of the substitutions seen in PR20: namely, S37N, I62V, I63P, A71V, I84V, and L90M.

A dimer dissociation constant of ∼30 nM measured for PR20 (Figure 3D) is at least 5-fold higher than that for PR, which is too small to measure accurately by enzyme kinetics (<5 nM, Figure 3D inset[4]). At a relatively low concentration, urea substantially decreases the catalytic activity as measured kinetically for PR20. The midpoint of maximum effect is observed at ∼0.75 M urea (UC$_{50}$) even in the presence of added sodium chloride, which is expected to stabilize the protease[32] (Figure 3E). This observation is due, at least in part, to an increase in K_m in the presence of urea, resulting in a strictly linear Michaelis−Menten plot (compare Figure 3A,3C). A similar effect of urea on K_m was previously observed for HIV-2 protease[23] but not for the protease of group N.[24] The effect of urea on PR20 as measured by the decrease in intrinsic fluorescence of PR20 in 50 mM sodium acetate buffer (Figure 3F) was qualitatively consistent with a significantly higher UC$_{50}$ of ∼1.7M, which is comparable to 1.8 M measured for PR
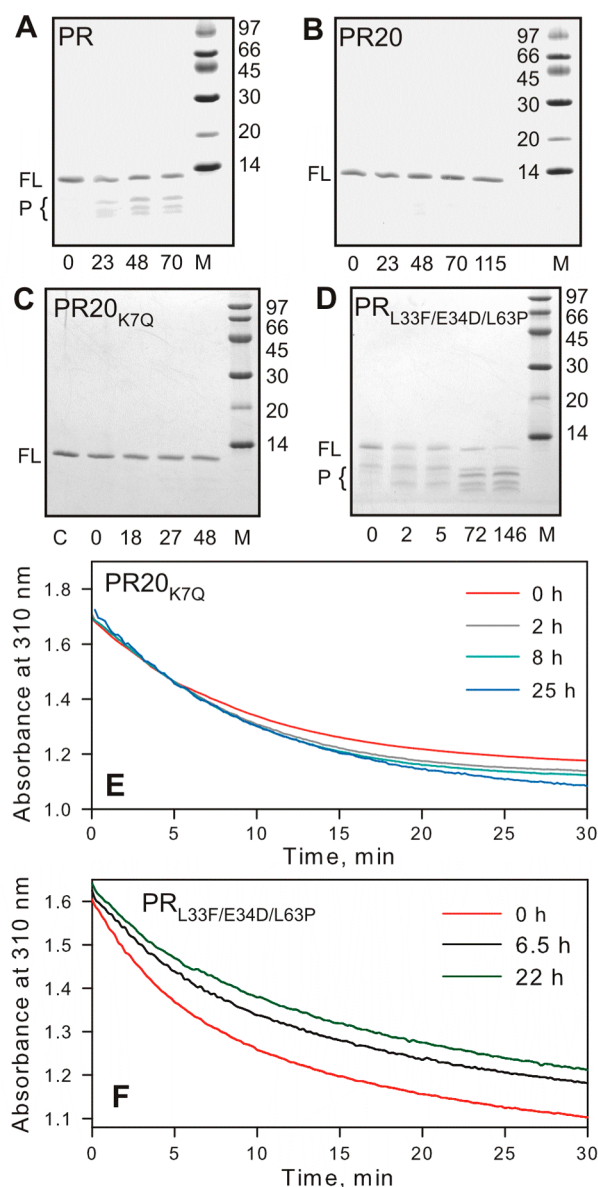
Figure 2. Time course of autoproteolysis of (A) PR, (B) PR20, (C) PR20_{K7Q,} and (D) PR_{L33F/E34D/L63P} at room temperature in 50 mM sodium acetate buffer, pH 5. Proteins were folded from 12 mM HCl by a quench protocol, as previously described,[25] to give a final concentration of 13 μM (as dimer) in 50 mM acetate, pH 5. Samples were withdrawn at the indicated times (in hours), mixed with gel loading buffer and analyzed by sodium dodecyl sulfate polyacrylamide gel electrophoresis (SDS-PAGE) (20% homogeneous PhastGel, GE Healthcare). FL and P designate full length protease and products of autoproteolysis, respectively. M denotes molecular weight markers in kDa. Numbers below the gels denote hours of incubation at room temperature. (C) and (E) show that PR20 bearing the wild-type residue in position 7 (K7Q) is equally resistant to autoproteolysis as PR20. Sample PR20_{K7Q} prior to initiating the assay is shown in lane C (panel C). (E and F) Time dependent decrease in protease mediated hydrolysis of substrate IV assayed at the indicated times at a final enzyme concentration of 440 nM for PR20_{K7Q} and 330 nM PR_{L33F/E34D/L63P} and final substrate concentration 380 μM, 28 °C. PR_{L33F/E34D/L63P} shows a significant decrease in catalytic activity with increasing time of incubation, consistent with appearance of products of autoproteolysis, unlike PR20 or PR20_{K7Q} (compare (B) and (C) with (D)). (D) and (F) demonstrate that mutations L33F and L63P are not responsible for the reduced rate of autoproteolysis seen with PR20 consistent with a rate comparable to wild-type PR.

(shown in Figure 3E[20]) in the same buffer, and presumably corresponds to a true unfolding process. The dependence of fluorescence on urea concentration was unchanged in the presence of 2 μM DRV, indicating no stabilization, in spite of an estimated K_L of 41 nM (Table 2).

Thermal Stability of PR20 and Its Monomeric T26A Mutant. Although the effect of urea concentration on denaturation is similar for PR and PR20, their sensitivity to thermal denaturation differs, such that the T_m for thermal denaturation of dimeric PR20, as measured by differential scanning calorimetry (DSC), is 6 °C higher than that for PR. In contrast, the T_m for the ternary PR20 dimer/inhibitor DRV complex is 11.1 °C lower than that of the corresponding PR dimer/DRV complex. This is a reflection of the drastically decreased binding affinity of PR20 for DRV (by a factor of at least 4000, Table 2).[9] We previously used the increase in T_m upon inhibitor binding to dimeric PR ($\Delta T_m = T_m$ of PR/PI complex $- T_m$ of PR without PI) as a semiquantitative indication of relative binding affinity;[21] thus for PR20, ΔT_m upon DRV binding is only 5.3 °C as compared to 22.4 °C for PR/DRV (Table 1A). Thermal denaturation of PR at pH ~5 is essentially irreversible,[21] whereas denaturation of PR20 and its DRV complex exhibited partial reversibility as shown by repeated DSC scans (Figure 5A), which is likely a result of its resistance to autoproteolysis.

To determine whether the thermal stability of PR20 is related to its tertiary fold together with interactions at its interface as a dimer or simply an effect of enhanced stability of the monomer fold, we created a PR20 monomer construct. The PR dimer in the absence of inhibitor is held together mainly through interactions of its conserved active-site residues Asp25-Thr26-Gly27 (fireman's grip) and the terminal 4 residues 1−4 and 96−99. On the basis of our earlier observation with PR that a single substitution mutation T26A dramatically shifts the monomer−dimer equilibrium toward the monomer ($K_d > 500$ μM),[4] we introduced the same mutation in PR20. Figure 4A shows a $^1H-^{15}N$ TROSY-HSQC spectrum of PR20_{T26A} acquired at a concentration of 100 μM (as monomer) at pH 5.8. Well dispersed signals characteristic of a folded structure were observed, analogous to that observed for PR_{T26A} monomer.[22] Similar to PR or its analogues, PR20 or PR20_{T26A} could not be subjected to column fractionation, coupled to light-scattering and RI detectors to determine its molecular status (dimer or monomer), because of their nonspecific interaction with column matrices. We estimate that the K_d for PR20_{T26A} is likely well above 500 μM, because the K_d for PR20 is at least 5-fold higher than that for PR (30 nM versus <5 nM).[4] Several lines of evidence support the conclusion that PR20_{T26A} is monomeric at the concentrations used in our experiments. (1) A spectrum of PR20_{T26A} reacquired at a 4-fold lower protein concentration exhibited peaks that clearly superimpose on those observed at 100 μM, indicating that PR20_{T26A} is monomeric even at 100 μM. (2) PR20_{T26A} is catalytically inactive when assayed at both 1 and 5 μM, consistent with its being a monomer (Figure 4B). (3) The DSC trace for PR20_{T26A} in the absence of inhibitor exhibits a low, broad thermal transition and decreased T_m relative to PR20, similar to observations (Figure 5B−D) with PR_{T26A} and other PR monomers.[21]

Having established that PR20_{T26A} is a monomer under the conditions of DSC (~14 μM as dimer) allowed us to compare the T_m of both PR and PR20 monomers under identical conditions. In the absence of an inhibitor, PR20_{T26A} exhibits a
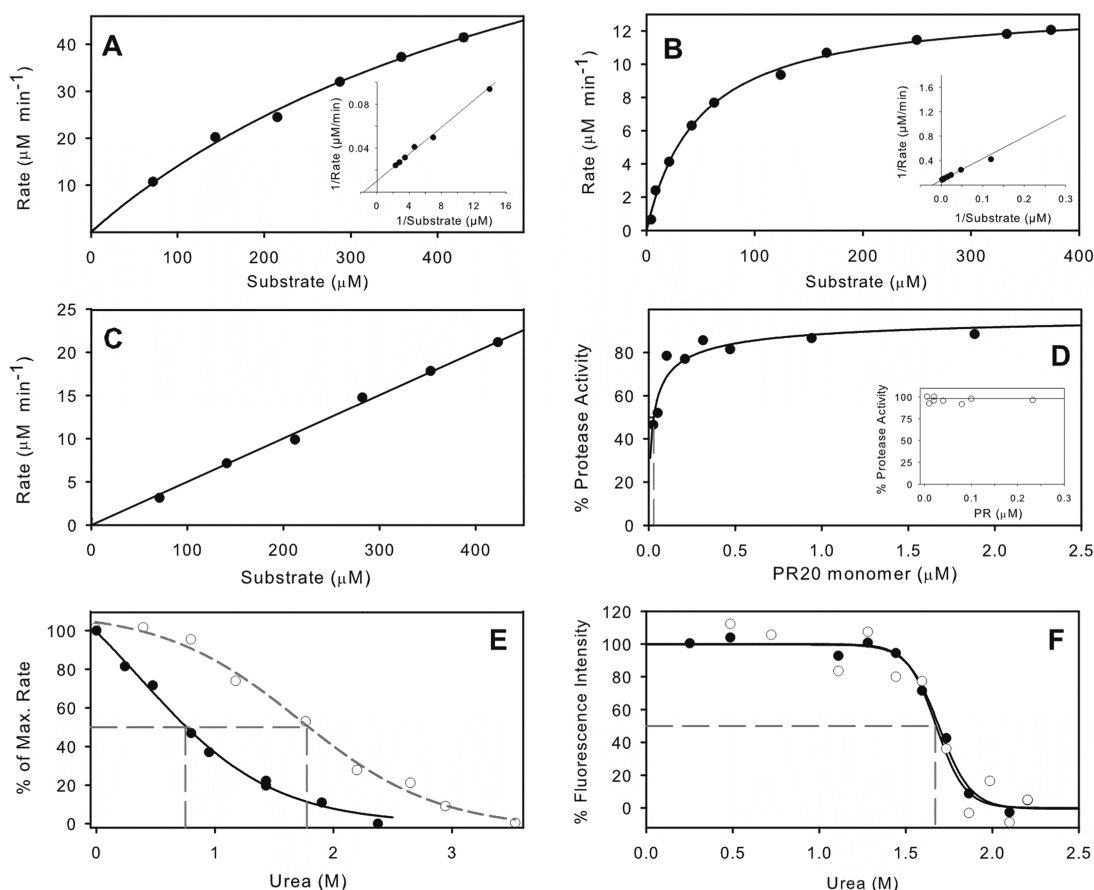
Figure 3. Kinetic properties of PR20 and comparison with PR. Michaelis−Menten kinetics for hydrolysis of substrate IV by 0.5 μM PR20 in 50 mM sodium acetate buffer, pH 5, containing 250 mM sodium chloride (A), and its hydrolysis under the same conditions[31] catalyzed by 80 nM PR. (B) Kinetic parameters for PR20 are $k_{cat.} = 196$ min^{-1} and $K_m \geq 533$ μM. For PR, $k_{cat.} = 174 \pm 3$ min^{-1} and $K_m = 48.2 \pm 3.1$ μM. Solid lines are based on curve fitting of the Michaelis−Menten equation to the data. Lineweaver−Burke plots are shown as insets. (C) The linear dependence of reaction rate for PR20 hydrolysis on substrate concentration, resulting from an increased K_m in the presence of 0.8 M urea under the same conditions as in (A). (D) Dependence of catalytic activity on the concentration of PR20 in the same buffer gives a K_d of 29 ± 10 nM (dashed gray line). For comparison, the inset shows that the K_d for PR is <5 nM under similar conditions.[20] (E) Effect of increasing urea concentration on hydrolysis of substrate IV by PR20 (●) and by PR[20] (○). (F) Effect of urea concentration on the intrinsic fluorescence of PR20 in 50 mM sodium acetate buffer, pH 5; data in the absence of inhibitor (●) and in the presence of 2 μM DRV (○). The urea concentrations at which 50% of the maximum effect (UC$_{50}$) is observed are indicated by dashed gray lines in (E) and (F).

Table 2. Thermodynamic Parameters for DRV Binding Determined by ITC[a]

protein	K_A (M^{-1})	K_L (nM)[b]	ΔH (kcal/mol)	$-T\Delta S$ (kcal/mol)	ΔG (kcal/mol)
PR[c]	2.2×10^{11}	0.005	−12.1	−3.1	−15.2
PR20[d]	$(2.45 \pm 0.59) \times 10^7$	41 ± 10	−7.6 ± 0.1	−2.6	−10.2
PR$_{D25N}$[e]	$(3.17 \pm 0.29) \times 10^5$	3200 ± 293	−5.8 ± 0.2	−1.8	−7.6
ANAM-11[d]	$(6.2 \pm 3.4) \times 10^8$	1.6 ± 0.8	−10.0 ± 0.07	−2.1	−12.1

[a]All titrations, unless noted otherwise, were performed in 50 mM sodium acetate buffer at pH 5.0 and 28 °C as described.[9] The thermodynamic parameters for PR20 and ANAM-11 are reported here for the first time. Other values incorporated in the table are solely for comparison. [b]Dissociation constant equal to $1/K_A$. [c]For wild-type PR, in 10 mM sodium acetate buffer, pH 5, at 20 °C.[38] [d]Reference 9. [e]Reference 21.

T_m that is 7.5 °C higher than that for PR$_{T26A}$. This is comparable to the 6 °C stabilization of the PR20 dimer and suggests that stabilization of the monomer fold may be a major factor contributing to the enhanced overall thermal stability of PR20 dimer. Interestingly, in the presence of excess DRV, the thermal transition for PR$_{T26A}$ becomes more pronounced (ΔH) and its T_m is increased by 3 °C. This suggests at least partial formation of a weak ternary PR$_{T26A}$ dimer/DRV complex promoted by DRV binding (Figure 5C). By contrast, no evidence for interaction of PR$_{T26A}$ with DRV or ternary complex formation was detected (Figure 5B and Table 1A).

This observation is consistent with both the lower affinity of PR20 for DRV and its somewhat higher dimer dissociation constant relative to PR. The nearly 4 orders of magnitude difference in affinity of DRV to PR20 relative to PR as measured by ITC (Table 2) corresponds to a ∼5 kcal/mol less favorable free energy, much of which is due to a less favorable ΔH (−5.8 as compared to −12 kcal/mol) for binding, consistent with fewer and/or weaker polar interactions with the inhibitor that can result from its expanded binding cavity and more open flap conformation.[13]
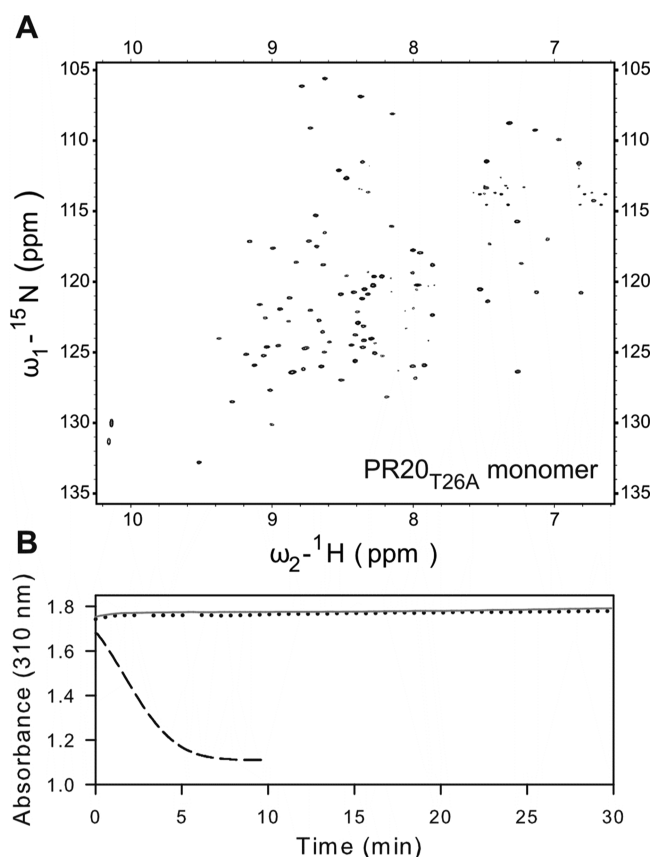
Figure 4. (A) 600 MHz $^1H-^{15}N$ TROSY-HSQC spectrum of freshly prepared uniformly ^{15}N- and ^{13}C-labeled PR20$_{T26A}$ (100 μM as monomer) in 20 mM sodium phosphate buffer, pH 5.8, 20 °C. A spectrum acquired using a 4-fold diluted sample (not shown) clearly superimposes on the one shown, indicating that no changes occurred in the monomer−dimer or tertiary fold status, and that the protein is all monomeric in conjunction with data shown in (B). (B) Activity assays with 360 μM substrate IV in 50 mM sodium acetate buffer, pH 5, containing 250 mM NaCl. Dotted black and solid gray lines are for 1 and 5 μM PR20$_{T26A}$ (as dimer), respectively. For comparison, the dashed line is for 300 nM active PR dimer shows depletion of substrate within 5 min.

Effect of Mutations at Sites of Autoproteolysis in PR20. The natural mutations L33F and L63P in PR20[19] occur at positions that are mutated (L33I and L63I) from the wild type to limit autoproteolysis of PR, and the presence of L63P provided a reasonable hypothesis to account for diminished autoproteolytic activity, because Pro occurs very rarely at the P1 position of substrates cleaved by PR.[33] To examine the effects of these mutations, we introduced L33F and L63P into a PR background (termed PR$_{L33F/L63P}$). The resultant construct failed to accumulate, likely due to rapid degradation in the *E. coli* expression system. Thus, we conclude that these two mutations by themselves do not impede autoproteolysis at their respective sites, likely requiring additional contributions from mutations at more-remote sites as seen in PR20 (Figure 1B). As it was not possible even after repeated attempts to isolate full length active PR$_{L33F/L63P}$, we introduced a conservative E34D substitution, which occurs rarely if at all at the P1′ position of a variety of PR substrates[33] and thus was thought unlikely to promote cleavage. This modification resulted in barely visible accumulation of PR$_{L33F/E34D/L63P}$, sufficient to purify and examine its thermal stability and inhibitor binding. This mutant
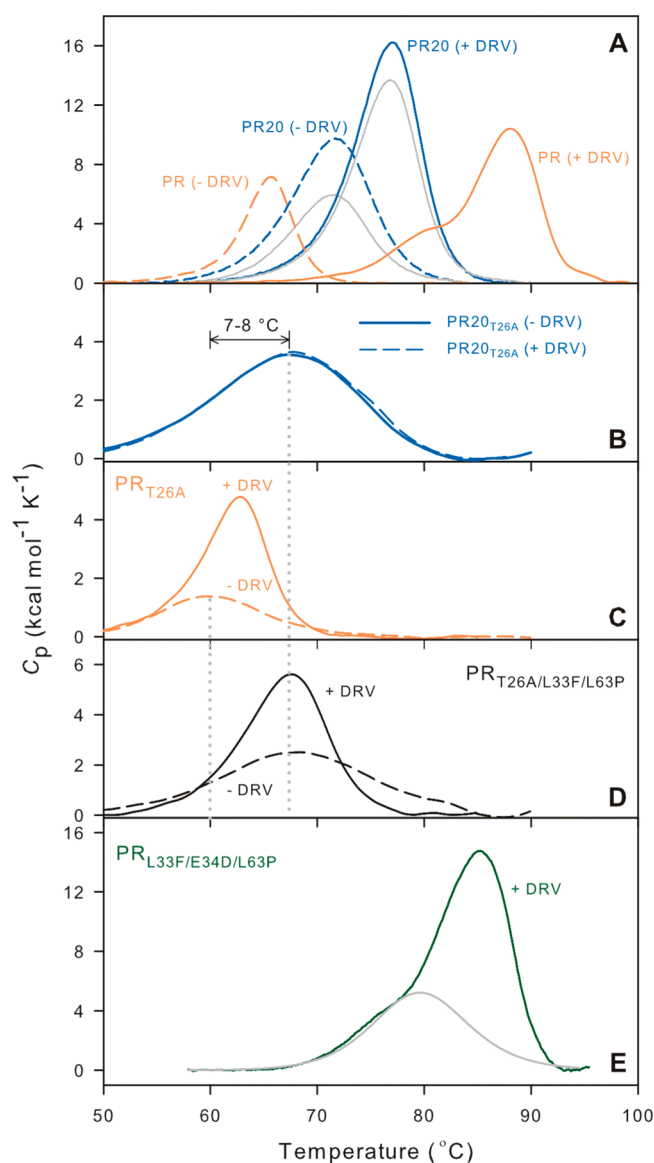

Figure 5. Differential scanning calorimetry of PR, PR20, and PR$_{L33F/E34D/L63P}$ dimers (A and E) and its corresponding monomers (B−D). Dashed and solid lines are thermal denaturation curves in the absence and presence of DRV, respectively. (A) Orange lines correspond to PR and blue to PR20. Traces shown in gray for PR20, obtained on a second scan of the DSC sample after completion of the initial scan, indicate partial reversibility of thermal melting in both the presence and absence of DRV. Data for PR, shown for comparison, are from.[21] Panels B−D show the effect of DRV on the thermal denaturation of PR20, PR, and PR$_{L33F/L63P}$ monomers bearing the T26A mutation. The absence of any effect of DRV on PR20$_{T26A}$ (B) indicates that this monomer likely does not form a complex with DRV. (E) Thermal denaturation of PR$_{L33F/E34D/L63P}$ dimer as its DRV complex (green). The curve in gray represents deconvolution of a transition with T_m = 79.7 °C, analogous to that seen in the biphasic DSC plot for PR (panel A). For values of T_m and ΔT_m derived from these plots, see Table 1A.

undergoes time dependent autoproteolysis comparable to or more than that of PR, concomitant with a decrease in catalytic activity within few hours (Figure 2D,2F). Major degradation products identified by ESI-MS correspond to well characterized self-cleavage sites for PR, between residues 33/34 and 63/64. Notably, thermal denaturation of PR$_{L33F/E34D/L63P}$ in the
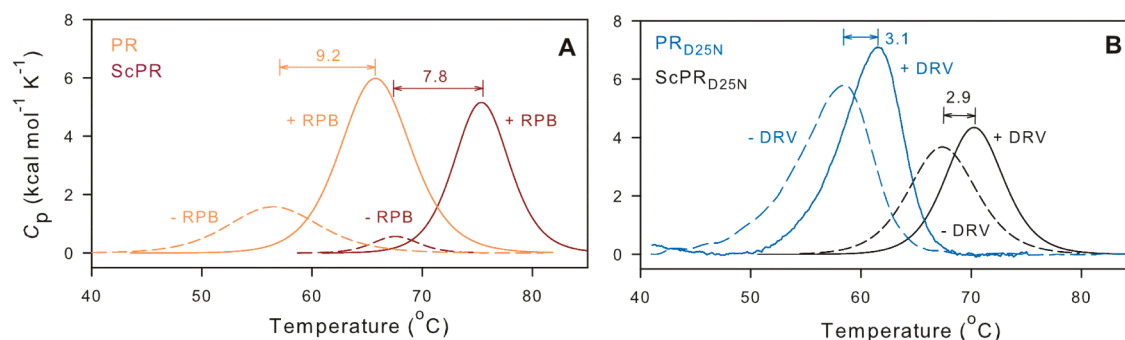
Figure 6. Effect of dimer stability on inhibitor binding and thermal denaturation of single-chain PR constructs ScPR (dark red) and ScPR$_{D25N}$ (black) in comparison with PR (orange) and PR$_{D25N}$ (blue) homodimers. Dashed and solid lines designate scans without inhibitor and with ~2-fold molar excess of inhibitor RPB or DRV relative to the respective proteases (as dimers). ΔT_m values shown for each pair of traces show the increase in T_m of each protein upon inhibitor binding. For experimental details, see the Materials and Methods section. Actual T_m values are given in Table 1B.

Table 3. Kinetic Data for PR-Catalyzed Hydrolysis of Synthetic Peptides Corresponding to Natural Cleavage Sites in HIV-1 Gag Polyprotein

substrate	sequence	enzyme	K_m (mM)	$k_{cat.}$ (s^{-1})	$k_{cat.}/K_m$ (mM^{-1} s^{-1})	activty (%) relative to PR	order of cleavage[a]
MA/CA	VSQNY↓PIVQ	PR	0.15	6.9	46.0		2
		PR20	0.91	3.0	3.2	7	1
CA/SP1	KARVL↓AEAMS	PR	0.02	0.9	42.4[b]		3
		PR20	0.11	0.1	1.2	2.8	3
SP1/NC	TATIM↓MQRGN	PR	0.10	6.7	67.0		1
		PR20	0.10	0.2	2.0	3.0	2
NC/SP2	ERQAN↓FLGKI	PR	0.17	0.15	0.9[c]		5
		PR20	0.23	0.0005	0.002	0.2	6
NC/SP2 mutant	ERRVN↓FLGKI	PR	nd[d]	nd	20.1[c]		4
		PR20	0.23	0.01	0.04	0.2	4
SP2/p6	RPQNF↓LQSRP	PR	0.48	0.4	0.8		6
		PR20	0.43	0.01	0.02	2.5	5

[a]Relative efficiency for cleavage of each substrate by the same enzyme, from highest (1) to lowest (6). [b]Reference 40. [c]Reference 39. [d]nd (not determined).

presence of a 2-fold excess of DRV gives a biphasic transition curve that closely resembles that of PR with a large ΔH and a T_m for the major transition that is only 2.7 °C lower than that for PR/DRV, and 10 °C higher than PR20/DRV complex (Figure 5E), indicative of tight binding to the inhibitor. Thus, L33F and L63P are also unlikely to play a significant role in the >4000-fold diminished DRV binding affinity of PR20 relative to PR, and mutations at other sites must be involved in drug resistance.

We also examined monomeric PR$_{T26A/L33F/L63P}$ to assess the effect of L33F and L63P on the thermal stability of the PR$_{T26A}$ monomer fold. In the absence of inhibitors, PR$_{T26A/L33F//L63P}$ exhibits a typically weak thermal transition but, surprisingly, with a T_m of ~68 °C that is very similar to that of PR20$_{T26A}$ and 7−8 °C higher than that of PR$_{T26A}$ (Figure 5D). The T_m of PR$_{T26A/L33F/L63P}$, like that of PR20, is essentially unaffected in the presence of a 2-fold molar excess of DRV; however, ΔH for this transition is increased by DRV, possibly due to weak interaction between the protease monomer and the inhibitor. Taken together, the present observations suggest that L33F and L63P in the wild-type context contribute significantly to stabilize the momomer fold while retaining the very high affinity for DRV. Thus, when extrapolated, the increased monomer stability of PR20 likely does not directly correlate with its drastically diminished affinity for DRV.

Relationship between Stability and Inhibitor Binding of Single-Chain PR Dimer. Because the monomer to dimer

equilibrium is slightly less favorable for PR20 than for PR, we assessed whether dimer stabilization exerts a significant effect on inhibitor binding. Thus, we examined two single-chain (Sc) dimers consisting of (1) two PR monomers both with active-site Asp25 residues, linked by a GGSSG sequence (ScPR) between the C terminus of one monomer and the N-terminus of the second monomer and (2) the corresponding single-chain dimer with both Asp25 residues mutated to Asn (ScPR$_{D25N}$). Because the affinity of inhibitors to PR20 is relatively low, we used conditions that would correspond to similar (nM to low μM) affinities (i.e., ScPR with a substrate (CA/SP1) analogue inhibitor, RPB, at pH 3.6, and ScPR$_{D25N}$ with DRV), which binds very poorly to PR$_{D25N}$, at pH 5.0. The T_m value (Table 1B) is 11 °C higher for ScPR than for homodimeric PR due to the stabilization provided by covalently linking two PR monomers. A comparable thermal stabilization of ~10 °C was observed for ScPR$_{D25N}$. Inhibitors designed to bind with high affinity to the stable mature PR dimer were shown to promote dimerization of protease precursors[34] and monomeric constructs,[4] which exhibit high K_d's. However, our present models, with moderate to weakly bound inhibitors, exhibit ΔT_m values on inhibitor binding (Table 1B and Figure 6) to the single-chain and homodimeric proteins that are the same within the accuracy of the DSC experiments (several of which exhibit low, broad thermal responses). Binding of RPB to both ScPR and PR at pH 3.6 gave $\Delta T_m(I)$ values of 8−9 °C, and binding of DRV to ScPR$_{D25N}$ and homodimeric PR$_{D25N}$ gave $\Delta T_m(I)$

values of ~3 °C. It is interesting to note that stabilization due to tethering (ΔT_m(Sc), Table 1B) is similar in the presence and absence of inhibitors. We conclude that the ΔT_m values observed with inhibitors that are not tightly bound may primarily reflect the disruption of direct interactions of the inhibitor with the active site and contiguous residues, which are essentially the same for both dimeric and single-chain constructs and do not induce significant remote changes that affect dimer stability. Because all currently available competitive inhibitors of PR bind only weakly to PR20, this lack of cooperative effects suggests that dimer stability may have, at best, only a limited role in PR20−inhibitor interactions.

Cleavage of Natural Substrates by PR20. Having defined some of the physical properties of PR20 and measured its kinetic parameters by using a chromogenic substrate, it was of interest to examine the ability of PR20, in comparison with PR, to catalyze cleavages in the Gag polyprotein ultimately required for the assembly of the virus particle. Catalytically competent, dimeric PR is released in a stepwise process (Figure 1A) involving intramolecular cleavages of the Gag−Pol (via transient dimers) (1) at the SP1/NC site followed by (2) between the TFR and PR domains at the N-terminus of PR, and subsequent intermolecular cleavage between PR and RT. Mature PR thus becomes available to catalyze release of structural proteins from the more prevalent Gag polyprotein by cleavages at SP1/NC followed by MA/CA and SP2/p6, and finally at the CA/SP1 and NC/SP2 sites.[2] Highly drug resistant protease mutants are compromised in their fitness to replicate due to reduced ability to cleave the polyprotein at these sites. PR20 exhibits significantly reduced catalytic efficiency for peptides corresponding to several of these cleavage sites at the high ionic strength optimal for oligopeptide substrate processing (Table 3), with a wide range of differences in $k_{cat.}/K_m$ between 0.2% and 7% relative to PR. K_m values for PR and PR20 are similar for SP1/NC, NC/SP2, and SP2/P6, such that differences in catalytic efficiency ($k_{cat.}/K_m$) on these substrates largely reflect differences in $k_{cat.}$. The catalytic efficiency decreases in the order shown in the last column and the trend for PR and PR20 remains the same. The substrates cluster into two groups: SP1/NC, MA/CA, and CA/SP1 (group 1) are hydrolyzed with relative efficiency, whereas NC/SP2 and SP2/P6 (group 2) are processed much less efficiently. Differences between the two groups are not clearly related to the temporal order of Gag processing. Thus, in group 1, the two best substrates for both enzymes, MA/CA and SP1/NC, represent early Gag cleavages, whereas cleavage at CA/SP1 (efficiency comparable to MA/CA) occurs later. Similarly, the early SP2/p6 cleavage is relatively inefficient. This leads us to speculate that the full-length Gag conformation(s) and the microenvironment in vivo also likely account for some of these differences.

The MA/CA cleavage in Gag is critical in that it must proceed almost to completion to ensure proper assembly of infectious virions.[2] In accordance, the MA/CA peptide is the best substrate examined for PR20, although not for PR. It exhibits the largest $k_{cat.}$ (only 2.3-fold slower than that for PR), which is offset by a high K_m. However, the local concentration of Gag is estimated to be ~4.4 mM within the immature virus particle[2] during or shortly after budding, when this cleavage probably occurs.[2,35] Thus, the high K_m for the MA/CA cleavage by mature PR20 may not present a serious disadvantage. In contrast to MA/CA, cleavage of the SP1/NC substrate by PR20 exhibits a moderately low $k_{cat.}$ and a low K_m, resulting in

overall catalytic efficiency that is close to that for MA/CA. The NC/SP2 substrate is cleaved by PR20 with the poorest efficiency. A double mutant containing polymorphisms QA → RV associated with drug resistance exhibited $k_{cat.}/K_m$ ~20-fold greater than for the wild-type substrate. Interestingly, A → V mutation at P2 of NC/SP2 site was shown to accompany the pair of PR mutations L33F/L63P in three HIV sequences derived from patients exhibiting multiple drug resistance.[36] However, the efficiency of PR20 relative to PR was unchanged for the mutant substrate. This suggests that the same pair of mutations present in Gag would confer equal advantages to PR and PR20. We speculate that substrate polymorphisms at other, as yet unidentified, sites in Gag and Gag−Pol may contribute to enhancing the catalytic efficiency of PR20 and viability of the virus.

■ CONCLUDING REMARKS

The mutant HIV protease PR20 bears multiple mutations that render it extremely resistant to PIs due to its weak binding to these inhibitors.[9,13] Although some of these mutations are known to compromise fitness, the virus is able to propagate. In fact, PR20 is a reasonably robust enzyme due to many secondary mutations that preserve its overall stability and function. (1) Mutations at or near sites of autoproteolysis acting in conjunction with other mutations in PR20 presumably increase the longevity of active PR20 in vivo by limiting degradation. (2) PR20 exhibits enhanced thermal stability relative to PR, which contributes to its functionality and viability of the virus (primarily through selection of mutations L33F and L63P). (3) PR20 cleaves peptides corresponding to sites in the Gag polyprotein essential for viral maturation. However, this catalysis is highly inefficient relative to PR. PR20 hydrolyzes a coevolved NC/SP2 substrate with ~20-fold increased efficiency relative to the wild-type site although not with the same efficiency as PR cleaving its natural NC/SP2 substrate. This is consistent with observations[37] that mutations affecting cleavage sites in the Gag and Gag−Pol can coevolve with a highly drug resistant PR bearing multiple mutations and provide a mechanism for partially circumventing inefficient catalysis. Lack of available sequence information spanning the Gag of the PR20 isolate precludes the identification of the role of such mutations in preserving the viability of this virus.

Our observation of a slightly compromised dimer dissociation constant for PR20 relative to PR, as well as comparable thermal stabilization of the PR20 monomer and dimer (6−7.5 °C), suggests that the enhanced thermal stability of this mutant protease over PR is predominantly or entirely the result of a more stable monomer fold. Thus, the enlarged binding cavity[13] and moderate weakening of interactions in regions contiguous to the active site and flaps may limit tight binding of inhibitors, while compensating changes elsewhere preserve the protein's overall structural integrity. The DRM, ANAM-11,[11] bears six mutations identical or similar to PR20 (L10I/F, M36I, L63P, A71V, I84V, and L90M) and exhibits similar properties of increased dimer dissociation ($K_d = 0.1 \pm 0.04$ μM)[9] along with moderately enhanced thermal stability (Table 1A). We speculate that monomer stabilization similar to that observed in the present study may be a characteristic of other DRMs and possibly constitutes an "evolutionary necessity" to permit the viability of highly drug resistant mutants. Because the protease precursor is monomeric and undergoes autoprocessing only via a transient dimer, mutations that structurally stabilize the monomer may also shift the equilibrium to favor precursor

monomers over transient dimers that can be trapped as inactive dimer/PI complexes. This could account in part for the failure of PIs to interact with the PR20 precursor to inhibit autoprocessing, thus making it impossible to isolate the precursor TFR-PR20, unlike TFR-PR, where extensive studies have been performed.[9] A monomer construct, $PR20_{T26A}$, shows no evidence for binding or partial dimerization in the presence of DRV under conditions where its pseudo-wild-type counterpart, PR_{T26A}, interacts weakly with this PI (Figure 5B,C). Substitutions of two PR20 residues, L33F and L63P, in PR or its monomeric model, PR_{T26A}, increase the monomer stability to an extent comparable with PR20 but permit effective DRV binding to a PR dimer. Thus, other mutations must contribute to the remarkable resistance to PIs exhibited by PR20. It is tempting to suggest that identification and targeting of such combinations of mutations could provide a potential strategy to overcome PI resistance in highly evolved PR variants or their precursors bearing multiple mutations.

■ AUTHOR INFORMATION

Corresponding Author

*John M. Louis. Address: Building 5, Room B2-29, LCP, NIDDK, NIH, Bethesda, MD 20892-0520. Tel: 301 594-3122. Fax: 301 480-4001. E-mail: johnl@intra.niddk.nih.gov.

Notes

The authors declare no competing financial interest.

■ ACKNOWLEDGMENTS

■ ABBREVIATIONS:

HIV-1, human immunodeficiency virus type 1; PR, mature HIV-1 protease containing the mutations Q7K, L33I, L63I, C67A, and C95A; PI, clinical protease inhibitor; DRM, drug resistance mutation (or drug resistant mutant), PR20, wild-type protease bearing 19 DRMs, Q7K, C67A, and C95A; DRV, darunavir; RPB, H-Arg-Val-Leu-(®)-Phe-Glu-Ala-Nle-NH2, (®) denotes a reduced peptide bond; DSC, differential scanning calorimetry; ITC, isothermal titration calorimetry; TROSY, transverse relaxation optimized spectroscopy; HSQC, heteronuclear single quantum coherence; K_d, protease dimer dissociation constant; K_L, ligand (inhibitor) dissociation constant; ScPR, single-chain PR

■ REFERENCES

(1) Oroszlan, S., and Luftig, R. B. (1990) Retroviral proteinases. *Curr. Top. Microbiol. Immunol. 157*, 153−185.

(2) Lee, S. K., Potempa, M., and Swanstrom, R. (2012) The choreography of HIV-1 proteolytic processing and virion assembly. *J. Biol. Chem. 287*, 40867−40874.

(3) Louis, J. M., Weber, I. T., Tozser, J., Clore, G. M., and Gronenborn, A. M. (2000) HIV-1 protease: maturation, enzyme specificity, and drug resistance. *Adv. Pharmacol. (San Diego, CA, U. S.) 49*, 111−146.

(4) Louis, J. M., Ishima, R., Torchia, D. A., and Weber, I. T. (2007) HIV-1 Protease: Structure, Dynamics, and Inhibition. *Adv. Pharmacol. (San Diego, CA, U. S.) 55*, 261−298.

(5) Pearl, L. H., and Taylor, W. R. (1987) A structural model for the retroviral proteases. *Nature 329*, 351−354.

(6) Wlodawer, A., and Erickson, J. (1993) Structure-based inhibitors of HIV-1 protease. *Annu. Rev. Biochem. 62*, 543−585.

(7) Johnson, V. A., Calvez, V., Gunthard, H. F., Paredes, R., Pillay, D., Shafer, R. W., Wensing, A. M., and Richman, D. D. (2013) Update of the drug resistance mutations in HIV-1: March 2013. *Top. Antivir. Med. 21*, 6−14.

(8) Agniswamy, J., and Weber, I. T. (2009) HIV-1 Protease: Structural perspectives on drug resistance. *Viruses 1*, 1110−1136.

(9) Louis, J. M., Aniana, A., Weber, I. T., and Sayer, J. M. (2011) Inhibition of autoprocessing of natural variants and multidrug resistant mutant precursors of HIV-1 protease by clinical inhibitors. *Proc. Natl. Acad. Sci. U. S. A. 108*, 9072−9077.

(10) Pieniazek, D., Rayfield, M., Hu, D. J., Nkengasong, J., Wiktor, S. Z., Downing, R., Biryahwaho, B., Mastro, T., Tanuri, A., Soriano, V., Lal, R., and Dondero, T. (2000) Protease sequences from HIV-1 group M subtypes A-H reveal distinct amino acid mutation patterns associated with protease resistance in protease inhibitor-naive individuals worldwide. HIV Variant Working Group. *AIDS 14*, 1489−1495.

(11) Muzammil, S., Ross, P., and Freire, E. (2003) A major role for a set of non-active site mutations in the development of HIV-1 protease drug resistance. *Biochemistry 42*, 631−638.

(12) Martin, P., Vickrey, J. F., Proteasa, G., Jimenez, Y. L., Wawrzak, Z., Winters, M. A., Merigan, T. C., and Kovari, L. C. (2005) "Wide-open" 1.3 A structure of a multidrug-resistant HIV-1 protease as a drug target. *Structure 13*, 1887−1895.

(13) Agniswamy, J., Shen, C. H., Aniana, A., Louis, J. M., Sayer, J. M., and Weber, I. T. (2012) HIV-1 protease with 20 mutations exhibits extreme resistance to clinical inhibitors through coordinated structural rearrangements. *Biochemistry. 51*, 2819−2828.

(14) Nijhuis, M., Schuurman, R., de Jong, J. D., Erickson, J., Gustchina, E., Albert, J., Schipper, P., Gulnik, S., and Boucher, C. A. (1999) Increased fitness of drug resistant HIV-1 protease as a result of acquisition of compensatory mutations during suboptimal therapy. *AIDS 13*, 2349−2359.

(15) Quiñones-Mateu, M. E., Weber, J., Rangel, H. R., and Chakraborty, B. (2001) HIV-1 Fitness and Antiviral Drug Resistance. *AIDS Rev 3*, 223−234.

(16) van Maarseveen, N. M., de Jong, J. D., Boucher, C. A., and Nijhuis, M. (2006) An increase in viral replicative capacity drives the evolution of protease inhibitor-resistant human immunodeficiency virus type 1 in the absence of drugs. *J. Acquired Immune Defic. Syndr. 42*, 162−168.

(17) Chang, M. W., and Torbett, B. E. (2011) Accessory mutations maintain stability in drug-resistant HIV-1 protease. *J. Mol. Biol. 410*, 756−760.

(18) Yanchunas, J., Jr., Langley, D. R., Tao, L., Rose, R. E., Friborg, J., Colonno, R. J., and Doyle, M. L. (2005) Molecular basis for increased susceptibility of isolates with atazanavir resistance-conferring substitution I50L to other protease inhibitors. *Antimicrob. Agents Chemother. 49*, 3825−3832.

(19) Dierynck, I., De Wit, M., Gustin, E., Keuleers, I., Vandersmissen, J., Hallenberger, S., and Hertogs, K. (2007) Binding kinetics of darunavir to human immunodeficiency virus type 1 protease explain the potent antiviral activity and high genetic barrier. *J. Virol. 81*, 13845−13851.

(20) Louis, J. M., Clore, G. M., and Gronenborn, A. M. (1999) Autoprocessing of HIV-1 protease is tightly coupled to protein folding. *Nat. Struct. Biol. 6*, 868−875.

(21) Sayer, J. M., Liu, F., Ishima, R., Weber, I. T., and Louis, J. M. (2008) Effect of the active-site D25N mutation on the structure, stability and ligand binding of the mature HIV-1 protease. *J. Biol. Chem. 283*, 13459−13470.

(22) Louis, J. M., Ishima, R., Nesheiwat, I., Pannell, L. K., Lynch, S. M., Torchia, D. A., and Gronenborn, A. M. (2003) Revisiting monomeric HIV-1 protease. Characterization and redesign for improved properties. *J. Biol. Chem. 278*, 6085−6092.

(23) Louis, J. M., Ishima, R., Aniana, A., and Sayer, J. M. (2009) Revealing the dimer dissociation and existence of a folded monomer of the mature HIV-2 protease. *Protein Sci. 18*, 2442−2453.

(24) Sayer, J. M., Agniswamy, J., Weber, I. T., and Louis, J. M. (2010) Autocatalytic maturation, physical/chemical properties, and crystal structure of group N HIV-1 protease: relevance to drug resistance. *Protein Sci. 19*, 2055−2072.

(25) Ishima, R., Torchia, D. A., and Louis, J. M. (2007) Mutational and structural studies aimed at characterizing the monomer of HIV-1 protease and its precursor. *J. Biol. Chem. 282*, 17190−17199.

(26) Delaglio, F., Grzesiek, S., Vuister, G. W., Zhu, G., Pfeifer, J., and Bax, A. (1995) NMRPipe: a multidimensional spectral processing system based on UNIX pipes. *J. Biomol. NMR 6*, 277−293.

(27) Goddard, T. D., and Kneller, D. G. (2010) *Sparky* 3, University of California, San Francisco, San Francisco, CA.

(28) Tozser, J., Blaha, I., Copeland, T. D., Wondrak, E. M., and Oroszlan, S. (1991) Comparison of the HIV-1 and HIV-2 proteinases using oligopeptide substrates representing cleavage sites in Gag and Gag-Pol polyproteins. *FEBS Lett. 281*, 77−80.

(29) Mildner, A. M., Rothrock, D. J., Leone, J. W., Bannow, C. A., Lull, J. M., Reardon, I. M., Sarcich, J. L., Howe, W. J., Tomich, C. S., and Smith, C. W. (1994) The HIV-1 protease as enzyme and substrate: mutagenesis of autolysis sites and generation of a stable mutant with retained kinetic properties. *Biochemistry 33*, 9405−9413.

(30) Tie, Y., Boross, P. I., Wang, Y. F., Gaddis, L., Hussain, A. K., Leshchenko, S., Ghosh, A. K., Louis, J. M., Harrison, R. W., and Weber, I. T. (2004) High resolution crystal structures of HIV-1 protease with a potent non-peptide inhibitor (UIC-94017) active against multi-drug-resistant clinical strains. *J. Mol. Biol. 338*, 341−352.

(31) Ishima, R., Torchia, D. A., Lynch, S. M., Gronenborn, A. M., and Louis, J. M. (2003) Solution structure of the mature HIV-1 protease monomer: insight into the tertiary fold and stability of a precursor. *J. Biol. Chem. 278*, 43311−43319.

(32) Szeltner, Z., and Polgar, L. (1996) Conformational stability and catalytic activity of HIV-1 protease are both enhanced at high salt concentration. *J. Biol. Chem. 271*, 5458−5463.

(33) Chou, K. C., Tomasselli, A. G., Reardon, I. M., and Heinrikson, R. L. (1996) Predicting human immunodeficiency virus protease cleavage sites in proteins by a discriminant function method. *Proteins 24*, 51−72.

(34) Agniswamy, J., Sayer, J. M., Weber, I. T., and Louis, J. M. (2012) Terminal Interface Conformations Modulate Dimer Stability Prior to Amino Terminal Autoprocessing of HIV-1 Protease. *Biochemistry 51*, 1041−1050.

(35) Adamson, C. S., and Freed, E. O. (2007) Human immunodeficiency virus type 1 assembly, release, and maturation. *Adv. Pharmacol. 55*, 347−387.

(36) Dam, E., Quercia, R., Glass, B., Descamps, D., Launay, O., Duval, X., Krausslich, H. G., Hance, A. J., and Clavel, F. (2009) Gag mutations strongly contribute to HIV-1 resistance to protease inhibitors in highly drug-experienced patients besides compensating for fitness loss. *PLoS. Pathog. 5*, e1000345.

(37) Kozisek, M., Henke, S., Saskova, K. G., Jacobs, G. B., Schuch, A., Buchholz, B., Muller, V., Krausslich, H. G., Rezacova, P., Konvalinka, J., and Bodem, J. (2012) Mutations in HIV-1 gag and pol compensate for the loss of viral fitness caused by a highly mutated protease. *Antimicrob. Agents Chemother. 56*, 4320−4330.

(38) King, N. M., Prabu-Jeyabalan, M., Nalivaika, E. A., Wigerinck, P., de Bethune, M. P., and Schiffer, C. A. (2004) Structural and thermodynamic basis for the binding of TMC114, a next-generation human immunodeficiency virus type 1 protease inhibitor. *J. Virol. 78*, 12012−12021.

(39) Feher, A., Weber, I. T., Bagossi, P., Boross, P., Mahalingam, B., Louis, J. M., Copeland, T. D., Torshin, I. Y., Harrison, R. W., and Tozser, J. (2002) Effect of sequence polymorphism and drug resistance on two HIV-1 Gag processing sites. *Eur. J. Biochem. 269*, 4114−4120.

(40) Ishima, R., Ghirlando, R., Tozser, J., Gronenborn, A. M., Torchia, D. A., and Louis, J. M. (2001) Folded monomer of HIV-1 protease. *J. Biol. Chem. 276*, 49110−49116.

(41) Ceccherini-Silberstein, F., Erba, F., Gago, F., Bertoli, A., Forbici, F., Bellocchi, M. C., Gori, C., D'Arrigo, R., Marcon, L., Balotta, C., Antinori, A., Monforte, A. D., and Perno, C. F. (2004) Identification of the minimal conserved structure of HIV-1 protease in the presence and absence of drug pressure. *AIDS 18*, F11−F19.

(42) Pettersen, E. F., Goddard, T. D., Huang, C. C., Couch, G. S., Greenblatt, D. M., Meng, E. C., and Ferrin, T. E. (2004) UCSF Chimera–a visualization system for exploratory research and analysis. *J. Comput. Chem. 25*, 1605−1612.